NIR-to-NIR Two-Photon Excited CaF_2:Tm^{3+},Yb^{3+} Nanoparticles: Multifunctional Nanoprobes for Highly Penetrating Fluorescence Bio-Imaging

Ning-Ning Dong,[†,‡] Marco Pedroni,[§] Fabio Piccinelli,[§] Giamaica Conti,[⊥] Andrea Sbarbati,[⊥] Juan Enrique Ramírez-Hernández,[∥] Laura Martínez Maestro,[†] Maria Carmen Iglesias-de la Cruz,[¶] Francisco Sanz-Rodriguez,[#] Angeles Juarranz,[#] Feng Chen,[‡] Fiorenzo Vetrone,[▲] John A. Capobianco,[▼] José García Solé,[†] Marco Bettinelli,[§] Daniel Jaque,[†,*] and Adolfo Speghini[§,*]

[†]Fluorescence Imaging Group, Departamento de Física de Materiales, Facultad de Ciencias, Universidad Autónoma de Madrid, 28049 Madrid, Spain, [‡]School of Physics, State Key Laboratory of Crystal Materials, Shandong University, Jinan 250100, China, [§]Dipartimento di Biotecnologie, Università di Verona and INSTM, UdR Verona, Ca'Vignal, Strada Le Grazie 15, 37134 Verona, Italy, [⊥]Dipartimento di Scienze Neurologiche, Neuropsicologiche, Morfologiche e Motorie, Università di Verona, Piazzale L.A. Scuro, 10-37134 Verona, Italy, [∥]Departamento de Investigación en Física, Universidad de Sonora, Hermosillo 5-88, 83190 México, [¶]Departamento de Fisiología, Facultad de Medicina, Universidad Autónoma de Madrid, C/Arzobispo Morcillo s/n 29029 Madrid, Spain, [#]Departamento de Biología, Facultad de Ciencias, Universidad Autónoma de Madrid, 28049 Madrid, Spain, [▲]Institut National de la Recherche Scientifique-Énergie, Matériaux et Télécommunications, Université du Québec, Varennes, QC J3X 1S2, Canada, and [▼]Department of Chemistry and Biochemistry, Concordia University, 7141 Sherbrooke Street West, Montreal, QC H4B 1R6, Canada

ABSTRACT In this study, we report on the remarkable two-photon excited fluorescence efficiency in the "biological window" of CaF_2:Tm^{3+},Yb^{3+} nanoparticles. On the basis of the strong Tm^{3+} ion emission (at around 800 nm), tissue penetration depths as large as 2 mm have been demonstrated, which are more than 4 times those achievable based on the visible emissions in comparable CaF_2:Er^{3+},Yb^{3+} nanoparticles. The outstanding penetration depth, together with the fluorescence thermal sensitivity demonstrated here, makes CaF_2:Tm^{3+},Yb^{3+} nanoparticles ideal candidates as multifunctional nanoprobes for high contrast and highly penetrating *in vivo* fluorescence imaging applications.

KEYWORDS: multifunctional nanoprobes · fluorescence bio-imaging · nanothermometers · near-infrared upconversion · calcium fluoride

Over the last years, the scientific community has witnessed countless developments in modern bio-imaging techniques. In particular, the combination of ultrafast laser oscillators, confocal microscopy, and biocompatible fluorescent nanoparticles has emerged as a powerful tool for high-resolution cellular and tissue imaging.[1−7] Although great efforts are still underway in the development of novel laser sources and optical microscopy techniques, it is widely assumed that the discovery of novel fluorescent nanoparticles is the key factor that could drive bio-imaging toward a new level of multifunctionality.[8−15] Among the various types of fluorescent nanoparticles that are currently used in bio-imaging, lanthanide-doped upconverting nanoparticles (UCNPs) are attracting considerable attention.[2,3,6,7,10,14−17] These nanoparticles can be multiphoton excited with near-infrared (NIR) light to generate emission at higher energies spanning the UV to the NIR. It has been demonstrated that they can lead to optical conversion efficiencies that are superior to those achieved by the widely used two-photon excited semiconductor quantum dots (QDs) and gold nanorods (GNRs).[18] In fact, due to the participation of real electronic states rather than virtual ones, the two-photon excited fluorescence in UCNPs does not require the use of high-intensity laser pulses but can be efficiently produced using inexpensive continuous wave laser sources.[19,20] Due to all of these outstanding features, UCNPs have quickly found uses as modern fluorescent biomarkers.[2,5−7,10,14,15] Indeed, the literature shows numerous examples of novel applications based on UCNPs, including intracellular imaging, diffuse tomography, and selective cancer cell detection.[2,3,14,15] The interest in UCNPs has been further enhanced due to the recent demonstration of their capability for intracellular thermal sensing based on the thermal-induced spectral changes in their fluorescence bands.[21−23] The spectral working range of UCNPs (excitation and emission ranges) is determined by the particular lanthanide dopant ions. Typically, erbium (Er) and

* Address correspondence to adolfo.speghini@univr.it, daniel.jaque@uam.es.

Received for review July 5, 2011 and accepted September 29, 2011.

Published online September 29, 2011
10.1021/nn202490m

ytterbium (Yb) codoping has been the pair of choice.[2,21,24,25] This is because the efficient Yb (donor) to Er (acceptor) energy transfer allows for NIR-to-visible optical conversion through a two-photon excitation mechanism. Furthermore, the Er^{3+} visible emissions lie in the spectral range where commercial multiphoton microscopes have their highest detection response. Nevertheless, the use of visible emitted wavelengths restricts their real application in bio-imaging due to their short tissue penetration depths (caused by tissue scattering and specific absorptions of tissue components such as melanin and hemoglobin).[26,27] To overcome this problem, other emitting ions could be used, with excited fluorescence bands lying within the so-called "biological window" (700−900 nm).[28] Previous works have already demonstrated that the Tm^{3+} and Yb^{3+} combination could be an interesting alternative.[29−32] Indeed, Tm^{3+}/Yb^{3+} codoped $NaYF_4$ nanoparticles have been already used for NIR *in vivo* imaging.[5]

Very recently, lanthanide-doped CaF_2 UCNPs have gained recognition due to their good infrared-to-visible upconversion fluorescence efficiencies.[33,34] These have been previously explained in terms of a combination of different factors. First, the low phonon energy of CaF_2 minimizes multiphonon de-excitation probabilities. Second, it is known that due to the presence of charge compensation effects, when doped with lanthanide ions, the CaF_2 network promotes the formation of pairs so that an effective reduction in the interatomic distance occurs, increasing the energy transfer rates (and hence the upconversion probability).[35] In addition, the stability and nonhygroscopic behavior of CaF_2 makes it an attractive material for nanoparticle fabrication. However, despite the promising preliminary results published on CaF_2:Tm^{3+},Yb^{3+} UCNPs, there are still some important open questions that should be answered before they can be used in real deep-tissue bio-imaging: their two-photon excited fluorescence efficiency (in comparison CaF_2:Er^{3+},Yb^{3+} UCNPs), their biocompatibility (not yet discussed for CaF_2 UCNPs), and most important, the actual tissue penetration depths that can be achieved based on their NIR emission. Finally, their potential use as nanothermometers (already demonstrated for $NaYF_4$:Er^{3+},Yb^{3+} UCNPs but never explored for Tm^{3+}-doped UCNPs) must be tested in order to endow their multifunctional character.

RESULTS AND DISCUSSION

The average particle sizes of the UCNPs, obtained from TEM measurements, are found to be typically 11 nm with a size dispersion of ±2 nm (see Figure 1a). All of the obtained UCNPs are cubic single phases, as revealed by a comparison of the XRPD patterns with the PDF no. 00-035-0816 card for cubic CaF_2 (Figure 1b). The presence of citrate groups at the surface of the UCNPs

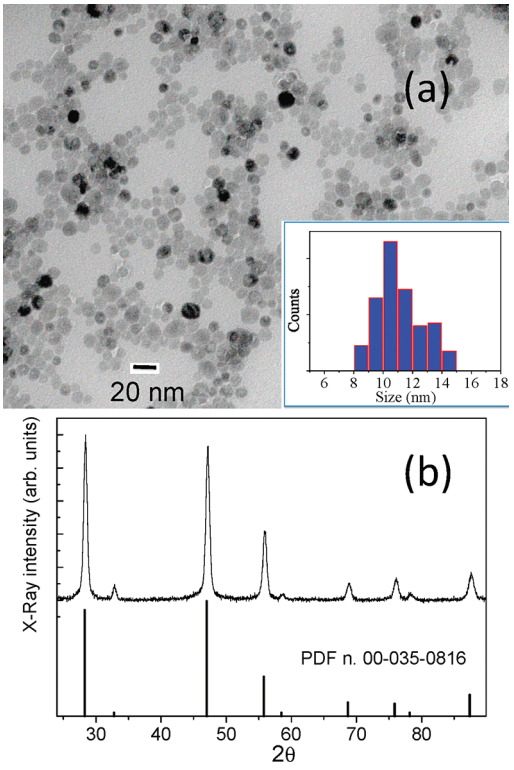

Figure 1. (a) TEM image and particle size distribution for the CaF_2:Tm^{3+},Yb^{3+} nanoparticles. Similar images are observed for the CaF_2:Er^{3+},Yb^{3+} nanoparticles. (b) X-ray diffraction pattern of the CaF_2:Tm^{3+},Yb^{3+} nanoparticles and PDF card no. 00-035-0816 (cubic CaF_2, $Fm\bar{3}m$ group). A similar pattern is found for the CaF_2:Er^{3+},Yb^{3+} nanoparticles.

was demonstrated by absorption spectra in the medium infrared region (see Figure S1, Supporting Information), which denoted the presence of the characteristic absorption bands of citrate groups (at 1400 and 1600 cm^{-1}).[36]

Figure 2 shows the two-photon excited emission spectra as obtained from both CaF_2:Er^{3+},Yb^{3+} and CaF_2:Tm^{3+},Yb^{3+} UCNPs. They were measured under identical experimental conditions (same focusing optics, same excitation pulse energy, and same collecting optics). The spectral extension of the biological window (limited by dispersion, hemoglobin, and melanin absorptions at short wavelengths and by water absorption at long wavelengths) is schematically indicated. Since the concentration of both types of UCNPs in the PBS solution (1 wt %) as well as the donor (Yb^{3+}) and acceptor (Er^{3+} or Tm^{3+}) dopant ion concentrations were identical, the data in Figure 2 constitute a comparison of the corresponding fluorescence efficiencies. It is clear that the optical conversion efficiency within the biological window is improved by more than 1 order of magnitude by using the Tm^{3+}-doped UCNPs instead of the Er^{3+}-doped ones. The two-photon conversion efficiency of the CaF_2:Tm^{3+},Yb^{3+} nanoparticles under investigation has been estimated (based on previous works and on their relative brightness measured in a confocal microscope) to be not higher than 1%.[18,37] Thus, high contrast multiphoton bio-images

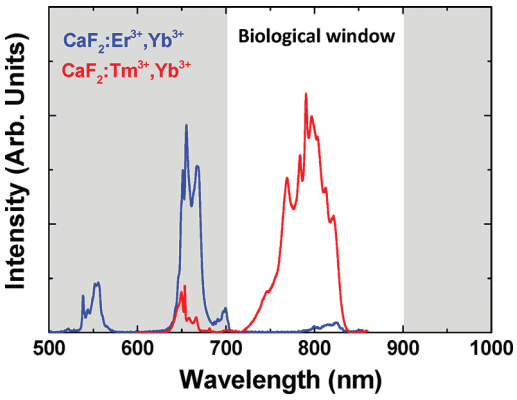

Figure 2. Two-photon excited emission spectra of CaF_2 nanoparticles codoped with Er^{3+},Yb^{3+} or with Tm^{3+},Yb^{3+}. Both spectra were obtained under 920 nm excitation and were corrected for the spectral system response. The spectra were not normalized, thus they provide a direct comparison of fluorescence efficiency. Note that in the biological window the Tm emission is more than 1 order of magnitude more intense than that of the Er emission.

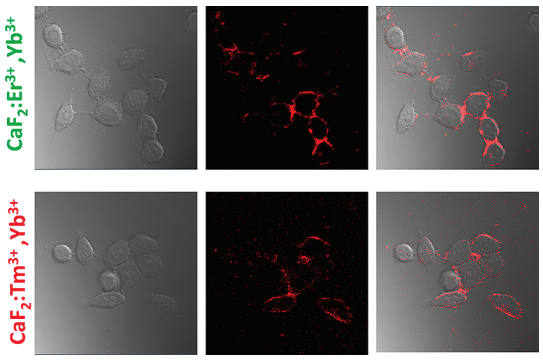

Figure 3. Top row shows (from left to right) the room temperature optical transmission images of HeLa cells incubated with the CaF_2:Er^{3+},Yb^{3+}/PBS solution, the two-photon fluorescence image, and the superimposed image. Bottom row shows (from left to right) the room temperature optical transmission images of HeLa cells incubated with the CaF_2:Tm^{3+},Yb^{3+}/PBS solution, the two-photon fluorescence image, and the superimposed image.

are expected to be obtained using the Tm^{3+}-doped UCNPs. To this respect, HeLa cancer cells were incubated with the CaF_2 UCNPs for 2 h at 37 °C. The initial colloidal suspension was additionally diluted by PBS (1:20 v/v). The successful cell marking by both CaF_2:Er^{3+},Yb^{3+} and CaF_2:Tm^{3+},Yb^{3+} UCNPs was verified using a fast multiphoton microscope, upon 920 nm excitation, and it is shown in Figure 3. The left column of Figure 3 demonstrates the optical transmission image of a group of HeLa cancer cells, whereas the corresponding fluorescence and superimposed images are displayed in the middle and right columns, respectively. No autofluorescence is observed. Thus, the results presented in Figure 3 confirm the potential use of both CaF_2:Er^{3+},Yb^{3+} and CaF_2:Tm^{3+},Yb^{3+} citrate-capped UCNPs in bio-imaging (*i.e.*, in cancer cell imaging). To the best of our knowledge, the images included in Figure 3 constitute the first bio-images obtained using CaF_2 UCNPs.

In order to determine whether the CaF_2 UCNPs can be used in real bio-imaging, we investigated the toxicity and cell viability of the HeLa cancer cells after treatment with the CaF_2 UCNPS. For this purpose, we used the MTT assay,[38] a method based on the activity of mitochondrial dehydrogenases, which will be functionally affected by UCNPs *in vitro*. The toxicity results are shown in Figure 4. As can be observed, no signal of additional toxicity with respect to the control HeLa cells was observed in our cell viability assays after 18 h of UCNP incubation. The toxicity of CaF_2 UCNPs was also tested in mesenchymal stem cells (a cell line not isolated by murine bone morrow) by using the same procedure as that applied to HeLa cells. In that case, we did not observe any noticeable toxic effect on the cells (in accordance with the results obtained with HeLa cells). Of course, it should be noted that the cell viability results presented here are only valid for CaF_2 citrate-capped nanoparticles. Thus, the good results obtained in terms of viability indicate that citrate capping makes CaF_2 UCNPs highly biocompatible. Similar experiments are being planned to check how the particular surface treatment effects determine the final biocompatibility of the CaF_2 nanoparticles.

Due to the significant Tm^{3+} NIR fluorescence with respect to the Er^{3+} one, a much deeper tissue penetration depth is expected using Tm^{3+}-doped UCNPs than for the Er^{3+}-doped ones. Figure 5a presents a schematic representation of the experimental setup used to compare the tissue penetration depths achievable using both CaF_2:Er^{3+},Yb^{3+} and CaF_2:Tm^{3+},Yb^{3+} UCNPs. The solution containing the UCNPs was placed in the same confocal microscope as the one used for Figure 2, but in this case, a phantom tissue with a variable thickness was placed between the colloidal suspension and the focusing/collecting microscope objective. This setup allowed us to measure the two-photon excited fluorescence for different tissue thickness by simply translating the colloidal suspension. The phantom tissue used in this work consists of a scattering medium (such as agar) containing several absorbing components (India ink and olive oil).[39−42] The ratio between the different components was adjusted in order to reproduce the main features of the absorption spectrum of human skin: high optical extinction coefficients (>8 cm^{-1}) in the visible region due to the presence of melanin and hemoglobin; a background absorption/extinction coefficient close to 6 cm^{-1} in the 700−900 nm range, due to scattering; and relevant absorption above 900 nm, due to the presence of water. All of these features have been well reproduced by our phantom tissue, as can be observed from the extinction spectrum shown in Figure 5b. For the sake of comparison, Figure 5c shows the variation of the collected two-photon excited fluorescence intensity as a function of the tissue thickness for the two different UCNP solutions (CaF_2:Er^{3+},Yb^{3+} and CaF_2:Tm^{3+},Yb^{3+}).

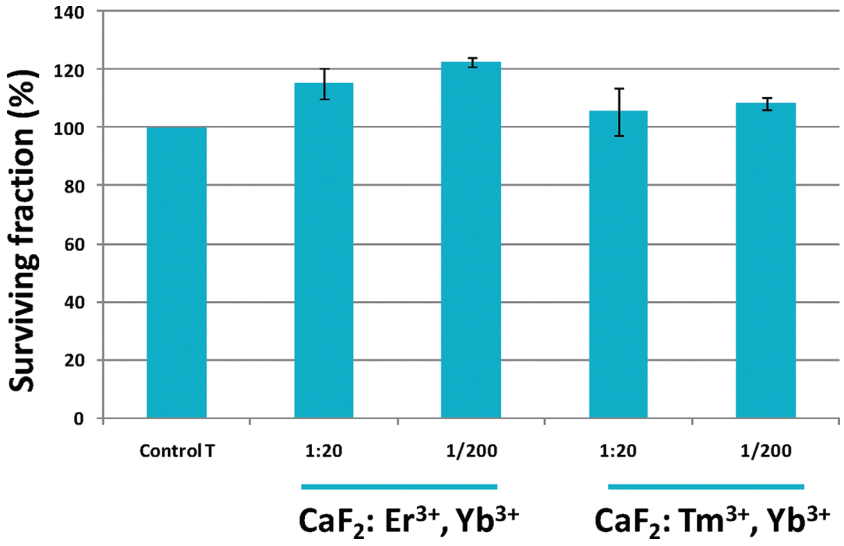

Figure 4. Percent survival of HeLa cell line incubated for a period of 18 h with different concentrations of CaF_2 UCNPs codoped with Er^{3+}/Yb^{3+} and Tm^{3+}/Yb^{3+} ions. Each point corresponds to the mean value ± SD from three different experiments.

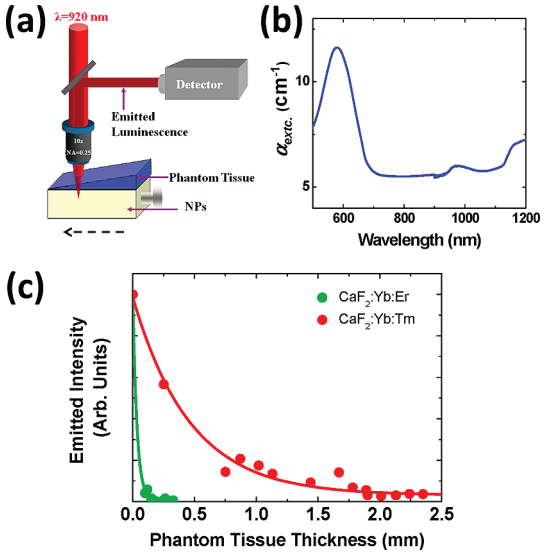

Figure 5. (a) Schematic representation of the experimental setup used to determine the penetration depths of two-photon excited CaF_2 nanoparticles. (b) Extinction spectrum of the phantom tissue used throughout this work. (c) Measured intensity at emission wavelengths of 655 nm (green dots) and 790 nm (red dots) for the CaF_2:Er^{3+},Yb^{3+} and CaF_2:Tm^{3+},Yb^{3+} nanoparticles, respectively, as a function of the phantom tissue thickness.

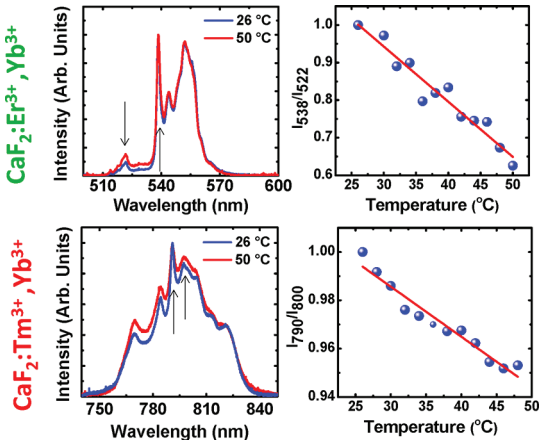

Figure 6. Two-photon excited emission spectra at two different temperatures as obtained from the Er^{3+}/Yb^{3+} and Tm^{3+}/Yb^{3+} codoped CaF_2 UCNPs (left side, top and bottom rows, respectively). The temperature dependence of the ratio between the fluorescence lines indicated by arrows on the spectra is shown in the right column. Dots are experimental data, and solid lines are guides for the eyes.

The emission wavelengths used for these measurements were 655 and 790 nm for the Er^{3+}/Yb^{3+} and Tm^{3+}/Yb^{3+} codoped CaF_2 UCNPs, respectively (*i.e.*, those leading to the maximum emitted intensity for each system). It is clear that, although the collected emission intensity drastically decreases with increasing phantom tissue thickness, appreciable fluorescence signals for the two solutions could still be obtained. However, in the case of the CaF_2:Tm^{3+},Yb^{3+} UCNPs, a fluorescence signal could still be observed up to a tissue thickness close to 2 mm. In fact, this penetration depth is comparable to the one recently achieved using two-photon excited NIR CdTe QDs (approximately 1.8 mm) (Maestro *et al.*, unpublished data). On the other hand, the visible emission generated by the CaF_2:Er^{3+},Yb^{3+} UCNPs is completely attenuated at a much shorter distance of 0.3 mm, that is, 6 times lower than that achieved using the 800 nm emission of Tm^{3+}. It is important to remark that the data included in Figure 5c represent he first direct measurement showing how the optical penetration depth in tissues is substantially improved by replacing the visible emitting Er^{3+} ions for the near-infrared emitting Tm^{3+} ones. In other words, data of Figure 5c clearly establish that the CaF_2:Tm^{3+},Yb^{3+} UCNPs are ideal for deep-tissue bio-imaging applications.

Moreover, Er^{3+}/Yb^{3+} codoped UCNPs are interesting not only because of their strong two-photon excited visible fluorescence but also because of the thermal sensitivity of their fluorescence that allows their use as nanothermometers, as already demonstrated for $NaYF_4:Er^{3+},Yb^{3+}$ UCNPs. Indeed, we have verified that a similar behavior exists in the $CaF_2:Er^{3+},Yb^{3+}$ UCNPs. The top row in Figure 6 presents the two-photon emission spectra of $CaF_2:Er^{3+},Yb^{3+}$ UCNPs as obtained at two different temperatures. A clear change in the relative intensity of the Er^{3+} ion emissions centered at 520 and 540 nm was observed due to the thermal coupling between the corresponding $^2H_{11/2}$ and $^2S_{3/2}$ emitting excited states. This ratio decreases monotonously with temperature, as can be observed on the graph at the top right quadrant of Figure 6, so that the experimental determination of this ratio gives a direct temperature measurement. Similar experiments were carried out with the $CaF_2:Tm^{3+},Yb^{3+}$ UCNPs, and the obtained results are shown in the bottom row of Figure 6. We have found that the ratio between the different fluorescence lines constituting the 800 nm fluorescence band of Tm^{3+} ions is remarkably modified by the temperature. This is explained by taking into account that these fluorescence lines are generated from thermally coupled sub-Stark energy levels belonging to the $^3H_4$ excited state of the Tm^{3+} ions. The most evident change has been observed between the fluorescence lines at 790 and 800 nm. Indeed, the ratio between the corresponding peak emitting intensities decreases monotonously with temperature, which can thus be used for thermal sensing. The data included in Figure 6 clearly indicate that $CaF_2:Tm^{3+},Yb^{3+}$ UCNPs can also be used as nanothermometers. The relative thermal-induced change in the ratio between the fluorescence intensities at 790 and 800 nm is lower than that obtained for $CaF_2:Er^{3+},Yb^{3+}$ UCNPs. Nevertheless, due to the much higher overall emitted intensity, the experimental error in the determination of fluorescence ratios within the Tm^{3+} band is improved with respect to the $CaF_2:Er^{3+},Yb^{3+}$ UCNPs, such that the final thermal sensitivities achievable from both systems are comparable.

CONCLUSIONS

In summary, we have performed the first cellular imaging experiments using $CaF_2:Er^{3+},Yb^{3+}$ and $CaF_2:Tm^{3+},Yb^{3+}$ UCNPs. These results together with the absence of cytotoxicity in the incubated cells make these nanoparticles excellent biocompatible probes. In addition, on the basis of the efficient NIR emission of Tm^{3+} ions, we have clearly demonstrated that $CaF_2:Tm^{3+},Yb^{3+}$ UCNPs lead to a much deeper penetration imaging power than that of $CaF_2:Er^{3+},Yb^{3+}$ UCNPs. As the $^3H_4 \rightarrow {}^3H_6$ transition of Tm^{3+} ions is sensitive to temperature changes, we also demonstrated the ability of $CaF_2:Tm^{3+},Yb^{3+}$ UCNPs as nanothermometers. These nanoparticles appear to be excellent multifunctional nanoprobes for high contrast and highly penetrating *in vivo* fluorescence imaging.

EXPERIMENTAL SECTION

Synthesis. The $CaF_2:Ln^{3+},Yb^{3+}$ (Ln = Er, Tm) UCNPs were synthesized by a single-step hydrothermal method using water as a solvent and citrate ions as capping agents. Reagent grade metal chlorides with Ca/Ln/Yb = 0.78:0.02:0.20 metal ratio were dissolved in 7 mL of deionized water with 20 mmol of sodium citrate. A proper amount of NH_4F was added in order to have a metal-to-fluoride molar ratio of 2.5. The transparent solution was heat treated in a Teflon-lined autoclave at 190 °C for 6 h. After centrifugation at 7000 rpm for 20 min, the UCNPs were collected. Colloidal dispersions for both $CaF_2:Tm^{3+},Yb^{3+}$ and $CaF_2:Er^{3+},Yb^{3+}$ UCNPs were prepared in PBS (1 wt %) without any evidence of precipitation over a period of several months.

Structural Characterization. X-ray powder diffraction (XRPD) patterns were measured using a Thermo ARL X'TRA powder diffractometer, equipped with a Cu anode X-ray source. The phase identifications were performed with PDF-4+ 2008 database provided by the International Centre for Diffraction Data (ICDD).

Electron Microscopy Characterization. Transmission electron microscopy (TEM) images were measured using a Philips Morgagni 268d electron microscope, operating at 80 KV. The powders were dispersed in water and deposited on a Formvar film-coated 150 mesh copper grid.

Spectroscopy Measurements. For two-photon fluorescence measurements, the colloidal solutions under study in this work were optically excited with 100 fs laser pulses with a 920 nm wavelength (with a repetition frequency of 80 MHz) by a mode-locked Ti:sapphire laser (Tsunami Spectra Physics). The laser beam was focused into the colloidal suspension by using 50× long working distance microscope objective (NA 0.55) of a Zeiss LSM510 microscope. The two-photon excited fluorescence was collected by using the same microscope objective and, after passing through several filters and apertures, was spectrally analyzed using a fiber-coupled high-resolution spectrometer. For thermal sensitivity experiments, the solution was mounted on a heating microscope with temperature control from 25 to 65 °C with a resolution of ±1 °C.

Toxicity Investigations. The toxicity of the CaF_2 nanoparticles was investigated in both HeLa and mesenchymal stem cells. The cell viability of those cells after treatment with the CaF_2 UCNPs was determined by the MTT assay,[37] a method based on the activity of mitochondrial dehydrogenases, which will be functionally affected by UCNPs *in vitro*. Following appropriate treatments, a 3-[4,5-dimethylthiazol-2-yl]-2,5-diphenyltetrazolium bromide (MTT) solution was added to each well at a concentration of 0.5 ng/mL, and plates were incubated at 37 °C for 2−3 h. The resulting formazan crystals were dissolved by the addition of DMSO, and absorbance was measured at 560 nm. The viability was also investigated by microscopy with a trypan blue exclusion test using a Neubauer chamber counter. Both methods concluded the same results.

Acknowledgment. This work was supported by the Universidad Autónoma de Madrid and Comunidad Autonoma de Madrid (Projects CCG087-UAM/MAT-4434 and S2009/MAT-1756), by the Spanish Ministerio de Educacion y Ciencia (MAT 2010-16161). J.A.C. thanks the Natural Sciences and Engineering Research Council (NSERC) of Canada and the Concordia

University Research Chairs program for funding. J.G.S. thanks the Spanish Minsterio de Educación for financial support for a research stay at Concordia University (ref PR2009-0040). Erica Viviani (Università di Verona, Verona, Italy) is acknowledged for expert technical support. The authors are grateful to Fondazione Cariverona (Verona, Italy) for financial support.

Supporting Information Available: Additional figure. This material is available free of charge *via* the Internet at http://pubs.acs.org.

REFERENCES AND NOTES

1. Ntziachristos, V.; Ripoll, J.; Wang, L. H. V.; Weissleder, R. Looking and Listening to Light: The Evolution of Whole-Body Photonic Imaging. *Nat. Biotechnol.* **2005**, *23*, 313–320.
2. Vetrone, F.; Naccache, R.; de la Fuente, A. J.; Sanz-Rodriguez, F.; Blazquez-Castro, A.; Rodriguez, E. M.; Jaque, D.; Sole, J. G.; Capobianco, J. A. Intracellular Imaging of HeLa Cells by Non-functionalized $NaYF_4$: Er^{3+}, Yb^{3+} Upconverting Nanoparticles. *Nanoscale* **2010**, *2*, 495–498.
3. Jiang, S.; Zhang, Y.; Lim, K. M.; Sim, E. K. W.; Ye, L. NIR-to-Visible Upconversion Nanoparticles for Fluorescent Labeling and Targeted Delivery of siRNA. *Nanotechnology* **2009**, *20*, 155101.
4. Xiong, L. Q.; Chen, Z. G.; Tian, Q. W.; Cao, T. Y.; Xu, C. J.; Li, F. Y. High Contrast Upconversion Luminescence Targeted Imaging *in Vivo* Using Peptide-Labeled Nanophosphors. *Anal. Chem.* **2009**, *81*, 8687–8694.
5. Nyk, M.; Kumar, R.; Ohulchanskyy, T. Y.; Bergey, E. J.; Prasad, P. N. High Contrast *In Vitro* and *In Vivo* Photoluminescence Bioimaging Using Near Infrared to Near Infrared Up-Conversion in Tm^{3+} and Yb^{3+} Doped Fluoride Nanophosphors. *Nano Lett.* **2008**, *8*, 3834–3838.
6. Chatteriee, D. K.; Rufalhah, A. J.; Zhang, Y. Upconversion Fluorescence Imaging of Cells and Small Animals Using Lanthanide Doped Nanocrystals. *Biomaterials* **2008**, *29*, 937–943.
7. Zhou, J.; Sun, Y.; Du, X. X.; Xiong, L. Q.; Hu, H.; Li, F. Y. Dual-Modality *In Vivo* Imaging Using Rare-Earth Nanocrystals with Near-Infrared to Near-Infrared (NIR-to-NIR) Upconversion Luminescence and Magnetic Resonance Properties. *Biomaterials* **2010**, *31*, 3287–3295.
8. Altinoglu, E. I.; Russin, T. J.; Kaiser, J. M.; Barth, B. M.; Eklund, P. C.; Kester, M.; Adair, J. H. Near-Infrared Emitting Fluorophore-Doped Calcium Phosphate Nanoparticles for *In Vivo* Imaging of Human Breast Cancer. *ACS Nano* **2008**, *2*, 2075–2084.
9. Chen, J.; Corbin, I. R.; Li, H.; Cao, W. G.; Glickson, J. D.; Zheng, G. Ligand Conjugated Low-Density Lipoprotein Nanoparticles for Enhanced Optical Cancer Imaging *in Vivo*. *J. Am. Chem. Soc.* **2007**, *129*, 5798–5799.
10. Hilderbrand, S. A.; Shao, F. W.; Salthouse, C.; Mahmood, U.; Weissleder, R. Upconverting Luminescent Nanomaterials: Application to *In Vivo* Bioimaging. *Chem. Commun.* **2009**, 4188–4190.
11. Idris, N. M.; Li, Z. Q.; Ye, L.; Sim, E. K. W.; Mahendran, R.; Ho, P. C. L.; Zhang, Y. Tracking Transplanted Cells in Live Animal Using Upconversion Fluorescent Nanoparticles. *Biomaterials* **2009**, *30*, 5104–5113.
12. König, K. Multiphoton Microscopy in Life Sciences. *J. Microsc.* **2000**, *200*, 83–104.
13. Rao, J. H.; Dragulescu-Andrasi, A.; Yao, H. Q. Fluorescence Imaging *in Vivo*: Recent Advances. *Curr. Opin. Biotechnol.* **2007**, *18*, 17–25.
14. Wang, F.; Banerjee, D.; Liu, Y. S.; Chen, X. Y.; Liu, X. G. Upconversion Nanoparticles in Biological Labeling, Imaging, and Therapy. *Analyst* **2010**, *135*, 1839–1854.
15. Wang, M.; Mi, C. C.; Wang, W. X.; Liu, C. H.; Wu, Y. F.; Xu, Z. R.; Mao, C. B.; Xu, S. K. Immunolabeling and NIR-Excited Fluorescent Imaging of HeLa Cells by Using $NaYF_4$:Yb,Er Upconversion Nanoparticles. *ACS Nano* **2009**, *3*, 1580–1586.
16. Haase, M.; Schäfer, H. Upconverting Nanoparticles. *Angew. Chem., Int. Ed.* **2011**, *50*, 5808–5829.
17. Wang, F.; Han, Y.; Lim, C. S.; Lu, Y.; Wang, J.; Xu, J.; Chen, H.; Zhang, C.; Hong, M.; Liu, X. Simultaneous Phase and Size Control of Upconversion Nanocrystals through Lanthanide Doping. *Nature* **2010**, *463*, 1061–1065.
18. Maestro, L. M.; Rodriguez, E. M.; Vetrone, F.; Naccache, R.; Ramirez, H. L.; Jaque, D.; Capobianco, J. A.; Sole, J. G. Nanoparticles for Highly Efficient Multiphoton Fluorescence Bioimaging. *Opt. Express* **2010**, *18*, 23544–23553.
19. Pedroni, M.; Piccinelli, F.; Passuello, T.; Giarola, M.; Mariotto, G.; Polizzi, S.; Bettinelli, M.; Speghini, A. Lanthanide Doped Upconverting Colloidal CaF_2 Nanoparticles Prepared by a Single-Step Hydrothermal Method: Toward Efficient Materials with Near Infrared-to-Near Infrared Upconversion Emission. *Nanoscale* **2011**, *3*, 1456–1460.
20. Boyer, J. C.; Cuccia, L. A.; Capobianco, J. A. Synthesis of Colloidal Upconverting $NaYF_4$: Er^{3+}/Yb^{3+} and Tm^{3+}/Yb^{3+} Monodisperse Nanocrystals. *Nano Lett.* **2007**, *7*, 847–852.
21. Vetrone, F.; Naccache, R.; Zamarron, A.; de la Fuente, A. J.; Sanz-Rodriguez, F.; Maestro, L. M.; Rodriguez, E. M.; Jaque, D.; Sole, J. G.; Capobianco, J. A. Temperature Sensing Using Fluorescent Nanothermometers. *ACS Nano* **2010**, *4*, 3254–3258.
22. Wade, S. A.; Collins, S. F.; Baxter, G. W. Fluorescence Intensity Ratio Technique for Optical Fiber Point Temperature Sensing. *J. Appl. Phys.* **2003**, *94*, 4743–4756.
23. Wang, S. P.; Westcott, S.; Chen, W. Nanoparticle Luminescence Thermometry. *J. Phys. Chem. B* **2002**, *106*, 11203–11209.
24. Yi, G. S.; Lu, H. C.; Zhao, S. Y.; Yue, G.; Yang, W. J.; Chen, D. P.; Guo, L. H. Synthesis, Characterization, and Biological Application of Size-Controlled Nanocrystalline $NaYF_4$: Yb,Er Infrared-to-Visible Up-Conversion Phosphors. *Nano Lett.* **2004**, *4*, 2191–2196.
25. Vetrone, F.; Naccache, R.; Mahalingam, V.; Morgan, C. G.; Capobianco, J. A. The Active-Core/Active-Shell Approach: A Strategy To Enhance the Upconversion Luminescence in Lanthanide-Doped Nanoparticles. *Adv. Funct. Mater.* **2009**, *19*, 2924–2929.
26. Frangioni, J. V. *In Vivo* Near-Infrared Fluorescence Imaging. *Curr. Opin. Chem. Biol.* **2003**, *7*, 626–634.
27. Marquez, G.; Wang, L. H. V.; Lin, S. P.; Schwartz, J. A.; Thomsen, S. L. Anisotropy in the Absorption and Scattering Spectra of Chicken Breast Tissue. *Appl. Opt.* **1998**, *37*, 798–804.
28. Weissleder, R. A Clearer Vision for *In Vivo* Imaging. *Nat. Biotechnol.* **2001**, *19*, 316–317.
29. Wong, H.-T.; Chan, H. L. W.; Hao, J. Towards Pure Near-Infrared to Near-Infrared Upconversion of Multifunctional GdF_3:Yb^{3+},Tm^{3+} Nanoparticles. *Opt. Express* **2010**, *18*, 6123–6130.
30. Jiang, T.; Qin, W.; Ding, F. Comparison of Ultraviolet Upconversion Luminescence between Thin Film and Bulk of Calcium Fluoride Co-Doped with Yb^{3+}/Tm^{3+} Ions. *J. Nanosci. Nanotechnol.* **2010**, *10*, 2013–2016.
31. Wang, F.; Liu, X. G. Upconversion Multicolor Fine-Tuning: Visible to Near-Infrared Emission from Lanthanide-Doped $NaYF_4$ Nanoparticles. *J. Am. Chem. Soc.* **2008**, *130*, 5642–5643.
32. Pandozzi, F.; Vetrone, F.; Boyer, J.-C.; Naccache, R.; Capobianco, J. A.; Speghini, A.; Bettinelli, M. A Spectroscopic Analysis of Blue and Ultraviolet Upconverted Emissions from $Gd_3Ga_5O_{12}$:Tm^{3+}, Yb^{3+} Nanocrystals. *J. Phys. Chem. B* **2005**, *109*, 17400–17405.
33. Kumar, A. G.; Chen, W. C.; Riman, E. R. *Optical Spectroscopy and Confocal Fluorescence Imaging of Upconverting Er^{3+}-Doped CaF_2 Nanocrystals*; American Institute of Physics: Melville, NY, ETATS-UNIS, 2007; Vol. 90.
34. Wang, G.; Peng, Q.; Li, Y. Upconversion Luminescence of Monodisperse CaF_2:Yb^{3+}/Er^{3+} Nanocrystals. *J. Am. Chem. Soc.* **2009**, *131*, 14200–14201.
35. Masahiko, I.; Christelle, G.; Yannick, G.; Kheirreddine, L.; Tsuguo, F.; Georges, B. Crystal Growth, Yb^{3+} Spectroscopy, Concentration Quenching Analysis and Potentiality of Laser Emission in $Ca_{1-x}Yb_x F_{2+x}$. *J. Phys.: Condens. Matter* **2004**, *16*, 1501.

36. Socrates, G. *Infrared and Raman Characteristic Group Frequencies*, 3rd ed.; John Wiley & Sons: New York, 2001.
37. Boyer, J.-C.; van Veggel, F. C. J. M. Absolute Quantum Yield Measurements of Colloidal $NaYF_4:Er^{3+}$, Yb^{3+} Upconverting Nanoparticles. *Nanoscale* **2010**, *2*, 1417–1419.
38. Denizot, F.; Lang, R. Rapid Colorimetric Assay for Cell Growth and Survival: Modifications to the Tetrazolium Dye Procedure Giving Improved Sensitivity and Reliability. *J. Immunol. Methods* **1986**, *89*, 271–277.
39. Flock, S. T.; Jacques, S. L.; Wilson, B. C.; Star, W. M.; Vangemert, M. J. C. Optical Properties of Intralipid—A Phantom Medium for Ligth Propagation Studies. *Lasers Surg. Med.* **1992**, *12*, 510–519.
40. Madsen, S. J.; Patterson, M. S.; Wilson, B. C. The Use of India Ink as an Optical Absorber in Tissue-Simulating Phantoms. *Phys. Med. Biol.* **1992**, *37*, 985–993.
41. Cubeddu, R.; Pifferi, A.; Taroni, P.; Torricelli, A.; Valentini, G. Time-Resolved Imaging on a Realistic Tissue Phantom: μ_s' and μ_a Images *versus* Time-Integrated Images. *Appl. Opt.* **1996**, *35*, 4533–4540.
42. Kobayashi, M.; Ito, Y.; Sakauchi, N.; Oda, I.; Konishi, I.; Tsunazawa, Y. Analysis of Nonlinear Relation for Skin Hemoglobin Imaging. *Opt. Express* **2001**, *9*, 802–812.